Efficient computation of three-dimensional flow in helically corrugated hoses including swirl

EINDHOVEN UNIVERSITY OF TECHNOLOGY
Department of Mathematics and Computer Science

CASA-Report 09-16
May 2009

Efficient computation of three-dimensional flow in helically corrugated hoses including swirl

by

B.J. van der Linden, E. Ory, J.A.M. Dam,
A.S. Tijsseling, M. Pisarenco

Centre for Analysis, Scientific computing and Applications
Department of Mathematics and Computer Science
Eindhoven University of Technology
P.O. Box 513
5600 MB Eindhoven, The Netherlands
ISSN: 0926-4507

EFFICIENT COMPUTATION OF THREE-DIMENSIONAL FLOW IN HELICALLY CORRUGATED HOSES INCLUDING SWIRL

Bas J. van der Linden[*]
CASA[†]
Department of Mathematics
Technische Universiteit Eindhoven
Eindhoven, The Netherlands
Email: b.j.v.d.linden@tue.nl

Emmanuel Ory
Single Buoy Mooring Offshore
Monaco, Monaco
Email: emmanuel.ory@sbmoffshore.com

Jacques Dam
Stork Inoteq
Amsterdam, The Netherlands
Email: jacques.dam@stork.com

Arris S. Tijsseling
CASA
Department of Mathematics
Technische Universiteit Eindhoven
Eindhoven, The Netherlands
Email: a.s.tijsseling@tue.nl

Maxim Pisarenco
CASA
Department of Mathematics
Technische Universiteit Eindhoven
Eindhoven, The Netherlands
Email: m.pisarenco@tue.nl

ABSTRACT

In this article we propose an efficient method to compute the friction factor of helically corrugated hoses carrying flow at high Reynolds numbers. A comparison between computations of several turbulence models is made with experimental results for corrugation sizes that fall outside the range of validity of the Moody diagram. To do this efficiently we implement quasi-periodicity. Using the appropriate boundary conditions and matching body force, we only need to simulate a single period of the corrugation to find the friction factor for fully developed flow.

A second technique is introduced by the construction of an appropriately twisted wedge, which allows us to furthermore reduce the problem by a further dimension while accounting for the Beltrami symmetry that is present in the full three-dimensional problem. We make a detailed analysis of the accuracy and time-saving that this novelty introduces.

We show that the swirl inside the flow, which is introduced by the helical boundary, has a positive effect on the friction factor. Furthermore, we give a prediction for which corrugation angles the assumption of axisymmetry is no longer valid. It then has to make place for Beltrami-symmetry if accurate results are required.

1 INTRODUCTION

This article studies the computation of friction factors of corrugated hoses for turbulent flow. The friction factor or, equivalently, the head loss of a hose is an important design characteristic, that is used in engineering applications to make important design decisions such as the required power of the pumps, that drive the flow, and the size of the hose's diameter.

When flexible hoses have to resist high pressure or temperature loads, the hose structure needs to be reinforced. Such reinforcement, especially when it needs to cover greater lengths, typically means winding a metal wire or other strong and thin material in a spiral around a flexible hose, made of fabric. This reinforcement changes the internal geometry of the hose, causing corrugations that strongly affect the flow in the hose.

[*]Please send all communication to this author.
[†]Centre for Analysis, Scientific Computing and Applications.

If the corrugation is small with respect to the hose's diameter, it can be treated in the same way as conventional surface roughness as long as it is taken into account, that the roughness is not random but regular [1]. The Moody diagram [2] — or more conveniently the equivalent explicit formulas as listed in [3] — can be used to reliably estimate the hose's performance. If the relative roughness exceeds 3%, however it is known that the Moody diagram is no longer applicable as the shape of the roughness becomes important. For the hoses of our interest, the corrugation was 5–10% of the diameter, which means that for each different shape of the corrugation the friction factor versus Reynolds number curve needs to be computed. At a design stage, this could involve large families of hose designs and so the computation of the friction factor must be efficient.

The shape of the cross section of the corrugation matters in more than one way. First of all, the size of the corrugation is so large that the flow near the wall is visibly affected. The flow will detach behind the corrugations, creating vortices in the troughs of the corrugation. At other points the flow will reattach, implying a stagnation point with a high pressure zone around it. Then, where the protrusion of the corrugation is the greatest,s the flow will locally contract and an underpressure will be created.

The spiral shape of the corrugations, that are discussed in this article, have also a macroscopic effect on the flow. Because the pressure forces on the wall align with the normal to the wall, and the wall has a helical structure, the counterforce exerted by the wall on the liquid has an azimuthal component. In this way the spiral shape of the corrugation causes the flow to swirl, which in turn affects the friction factor. Unfortunately, these observations mean that we need to know the flow at a small scale and in all three dimensions, even when we are eventually only interested in a global quantity, a single number: the friction factor.

In this paper we investigate how we can efficiently compute the friction factor of a helically corrugated hose without getting stuck in lengthy computer simulations. The question, how we can compute a global quantity both reliably and in finite time, even if it so much depends on knowing the local, small scale structure of the flow, is answered in three steps.

After introducing the governing equations in the next section, we first reduce the problem by a whole spatial dimension by making use of the fact that a fully developed flow is quasi-periodic. This first step is the most important as it means that we can predict the performance of a hose of a few hundred metres by only considering a geometry of a few centimetres in length. The second computational reduction is quite straightforward for annular corrugations, but the third step shows another dimension can be taken out of the geometry by using the flow's helical symmetry. This flow involves swirl, which is studied in the section before the conclusive last section.

Figure 1. Small section of a corrugated hose.

2 NUMERICAL SIMULATION OF TURBULENT FLOW IN HOSES

As we noted in the introduction, the observation, that the shape of the corrugation matters for the friction factor, means the flow needs to be known in full detail for an accurate prediction of the friction factor.

A small section of the type of hose that we wish to study is displayed in Figure 1. The diameter ranges from 10 cm to half a metre and the hoses are filled with a water-like liquid with speeds up to 5 to 10 m/s. With a density of 1000 kg/m^3 and viscosity of 1 mPa $\cdot$ s, the Reynolds number is $\mathrm{Re}_D = 10^6$, so deep in the turbulent region. The corrugation has a height of 1–2 cm and a spiral angle of only a few degrees.

The Reynolds number is too high to study the flow in every detail, for example with Direct Numerical Simulation (DNS). Rather the turbulence needs to be modelled and estimated. Fortunately, the Reynolds number is so elevated that we can use the so-called Reynolds Averaged Navier-Stokes approximation for the flow. For a complete understanding of the underlying processes reference [4] is recommended literature. A shorter (but less profound) road to the governing equations is given in [5], which we will follow here.

2.1 The Reynolds-Averaged Navier-Stokes equations

While the standard Navier-Stokes equations are equally valid for turbulent flows, the variations in the flow happen on such small length and time scales, that direct numerical simulation becomes prohibitively expensive. The computational cost in terms of number of operations of direct numerical simulation is estimated at Re^3 in [4]. For a Reynolds number of about one million this means that it is too costly on today's computer systems.

Rather than solving each small flow feature in full detail, we can take a stochastic view on the flow. After all, the averaged properties determine the flow characteristics for engineering applications. The full details of the flow is of no concern for the application that we are interested in. To that purpose we split the three speed components u_i, where the index i stands for the three spatial directions, i.e. $i \in \{1,2,3\}$ into an (time, space or ensemble) averaged speed $\overline{u}_i$ and a fluctuation u_i' as a deviation of that average. If we do the same for the pressure we find

$$u_i = \overline{u}_i + u_i' \quad \text{and} \quad p = \overline{p} + p'. \tag{1}$$

Substituting this into the standard Navier-Stokes equations, averaging those equations, and making use of the Boussinesq hypothesis yield the Reynolds Averaged Navier-Stokes (RANS) equations in the following form (see [5]):

$$\frac{\partial \overline{u}_i}{\partial x_i} = 0, \tag{2}$$

$$\rho \frac{\partial \overline{u}_i}{\partial t} + \rho \overline{u}_j \frac{\partial \overline{u}_i}{\partial x_j} = -\frac{\partial \overline{p}}{\partial x_i} + \frac{\partial}{\partial x_j}\left[2(\mu + \mu_T)\overline{S}_{ij} - \frac{2}{3}\rho k \delta_{ij}\right], \tag{3}$$

where the Reynolds averaged strain rate $\overline{S}_{ij}$ and turbulent kinetic energy k are defined by

$$\overline{S}_{ij} := \frac{1}{2}\left(\frac{\partial \overline{u}_i}{\partial x_j} + \frac{\partial \overline{u}_j}{\partial x_i}\right) \quad \text{and} \quad k := \overline{u_i' u_i'}. \tag{4}$$

Next to the strain rate, later we will also use the Reynolds stress tensor, which is defined as

$$\tau_{ij}^R := \rho \overline{u_i' u_j'} = 2\mu_T \overline{S}_{ij} - \tfrac{2}{3}\rho k \delta_{ij}, \tag{5}$$

where the second equality is a consequence of the Boussinesq hypothesis. We do not include an energy equation as we make the assumption that the flow is both incompressible and has uniform density, i.e. the density is not influenced by the temperature.

The turbulent viscosity μ_T, that appears in (3), is not a property of the fluid — unlike the dynamic viscosity μ — but rather is a property of the flow. It is left up to turbulence models to provide a good estimate of the turbulent viscosity, and therefore, we have a look at a selection of turbulence models next.

To make the computation of the friction factor of the corrugated hose independent of the underlying CFD solver used, we focused on widely available turbulence models. Given the range of Reynolds numbers, that we are interested in, this means using eddy-viscosity models, notably k-ε and variations thereof.

2.2 Turbulence models

The most widely implemented (and most widely tested) turbulence model is the so-called k-ε model. In the k-ε model [4,6], the turbulent viscosity is determined by two additional parameters: the turbulent kinetic energy k, that we already have introduced, and the turbulent dissipation rate ε. Since the low Reynolds number formulation, with a scaling function near the wall, tends to lead to numerical time integration difficulties, we use the high Reynolds number formulation:

$$\begin{aligned}
\rho \frac{\partial k}{\partial t} + \rho \overline{u}_j \frac{\partial k}{\partial x_j} &= \frac{\partial}{\partial x_j}\left[\left(\mu + \frac{\mu_T}{\sigma_k}\right)\frac{\partial k}{\partial x_j}\right] + \tau_{ij}^R \overline{S}_{ij} - \rho\varepsilon, \\
\rho \frac{\partial \varepsilon}{\partial t} + \rho \overline{u}_j \frac{\partial \varepsilon}{\partial x_j} &= \frac{\partial}{\partial x_j}\left[\left(\mu + \frac{\mu_T}{\sigma_\varepsilon}\right)\frac{\partial \varepsilon}{\partial x_j}\right] \\
&\quad + C_{\varepsilon 1}\frac{\varepsilon}{k}\tau_{ij}^R \overline{S}_{ij} - C_{\varepsilon 2}\rho\frac{\varepsilon^2}{k}.
\end{aligned} \tag{6}$$

The turbulent viscosity is then given by

$$\mu_T = C_\mu \rho \frac{k^2}{\varepsilon}. \tag{7}$$

In these equations the model parameters $C_{\varepsilon 1}$, $C_{\varepsilon 1}$, C_μ, σ_k and σ_ε are usually determined by fitting the model to measurement data. A commonly used model is Launder-Sharma [5] which defines these numbers as

$$\begin{gathered}
C_\mu = 0.09, \quad C_{\varepsilon 1} = 1.44, \quad C_{\varepsilon 2} = 1.92, \\
\sigma_k = 1.0, \quad \sigma_\varepsilon = 1.3.
\end{gathered} \tag{8}$$

The high Reynolds formulation cannot resolve the flow all the way to the wall, so wall functions have to be used. These wall functions resolve the inner part of the boundary layer. We discussed them extensively in [7]. Here, we only mention the main drawback of using wall functions: they are derived for straight walls with no adverse pressure gradient and they lack any theoretical basis to be applied outside these settings.

The second turbulence model, Wilcox's k-ω model [8], which is widely implemented solves some of the drawbacks of the k-ε model. Because it resolves the boundary layer by itself, it does not depend on wall functions. Furthermore, it has the benefit that it is numerically easier to integrate in time than the low Reynolds number k-ε model. It also uses the turbulent kinetic energy k as an extra variable, but rather uses the *specific dissipation*

of turbulence ω, defined as $\omega := \varepsilon/k$. The equations are

$$\begin{aligned}\rho\frac{\partial k}{\partial t}+\rho\overline{u}_j\frac{\partial k}{\partial x_j} &= \tau^R_{ij}\frac{\partial \overline{u}_j}{\partial x_j}-\rho\beta^* k\omega+\frac{\partial}{\partial x_j}\left[(\mu+\sigma^*_\omega\mu_T)\frac{\partial k}{\partial x_j}\right]\\ \rho\frac{\partial \omega}{\partial t}+\rho\overline{u}_j\frac{\partial \omega}{\partial x_j} &= \alpha\frac{\omega}{k}\tau^R_{ij}\frac{\partial \overline{u}_i}{\partial x_j}-\rho\beta\omega^2+\frac{\partial}{\partial x_j}\left[(\mu+\sigma_\omega\mu_T)\frac{\partial \omega}{\partial x_j}\right].\end{aligned} \tag{9}$$

Also, this model contains model parameters. In this case:

$$\alpha=\tfrac{5}{9},\quad \beta=\tfrac{3}{40},\quad \beta^*=\tfrac{9}{100},\quad \sigma_\omega=\tfrac{1}{2},\quad \sigma^*_\omega=\tfrac{1}{2}. \tag{10}$$

The turbulent dissipation rate can be found by $\varepsilon=\beta^*\omega k$ and the turbulent viscosity by $\mu_T=\rho k/\omega$. The boundary equations are $k=0$, while ω goes asymptotically to infinity for smooth walls, which makes the boundary condition dependent on the local mesh size near the wall. For rough walls (which we have in between the corrugations, see [7]) this is not the case and we can simply use $\omega=N\mu/k_s^2$ [9] with $N=2500$ and k_s the surface roughness height.

While the k-ω model performs better, when adverse pressure gradients are present, it performs worse than the k-ε model in the freestream. The third and final model that we consider is Menter's k-ω Shear-Stress Transport (SST) model [10]. It can be seen as a combination between the two previous models, where it uses the k-ω near the wall and k-ε away from the wall. This leads to much better results for adverse pressure gradients [11] and reattaching flows [12]. The equations are

$$\begin{aligned}\rho\frac{\partial k}{\partial t}+\rho\overline{u}_j\frac{\partial k}{\partial x_j} &= \frac{\partial}{\partial x_j}\left[(\mu+\sigma_k\mu_T)\frac{\partial k}{\partial x_j}\right]\\ &\quad+\tau^R_{ij}\overline{S}_{ij}-\beta^*\rho\omega k,\\ \rho\frac{\partial \omega}{\partial t}+\rho\overline{u}_j\frac{\partial \omega}{\partial x_j} &= \frac{\partial}{\partial x_j}\left[(\mu+\sigma_\omega\mu_T)\frac{\partial \omega}{\partial x_j}\right]+\\ &\quad\frac{C_\omega\rho}{\mu_T}\tau^R_{ij}\overline{S}_{ij}-\beta^*\rho\omega^2+2(1-f_1)\frac{\rho\sigma_{\omega2}}{\omega}\frac{\partial k}{\partial x_j}\frac{\partial \omega}{\partial x_j},\end{aligned} \tag{11}$$

where the blending function f_1 is defined by

$$\begin{aligned}f_1&=\tanh(\zeta_1^4),\\ \zeta_1&:=\min\left[\max\left(\frac{\sqrt{k}}{0.09\omega d},\frac{500\mu}{\rho\omega d^2}\right),\frac{4\rho\sigma_{\omega2}k}{\mathrm{CD}_{k\omega}d^2}\right],\\ \mathrm{CD}_{k\omega}&=\max\left[\frac{2\rho\sigma_{\omega2}}{\omega}\frac{\partial k}{\partial x_j}\frac{\partial \omega}{\partial x_j},10^{-20}\right].\end{aligned} \tag{12}$$

Here we use d for the distance to the nearest wall. The computation of the turbulent viscosity also becomes more complicated:

$$\mu_T=\frac{a_1\rho k}{\max(a_1\omega,f_2\|\nabla\times\overline{\mathbf{u}}\|)}, \tag{13}$$

with f_2 a second blending function:

$$f_2=\tanh\zeta_2^2,\ \zeta_2=\max\left(\frac{2\sqrt{k}}{0.09\omega d},\frac{500\mu}{\rho\omega d^2}\right). \tag{14}$$

2.3 Meshing

For computational fluid dynamics constructing a mesh is of the same importance as using the correct equations. For all viscous flow computations it is best that the mesh elements near the wall are aligned with the flow. But turbulence models such as k-ε or k-ω SST put additional constraints on the mesh size near the boundary.

The high Re k-ε model uses wall functions and is the more forgiving. Wall functions are semi-empirical expressions that model the viscosity-affected inner region of the boundary layer (the viscous sublayer and the buffer layer). The differential equations for k and ε are only responsible for the fully turbulent region (where the underlying assumptions for that model are valid). Without going into the details of the wall functions (see [7] for an extensive discussion), we only mention, that the size of the mesh perpendicular to the wall has to fall in a specific range:

$$50\le y^+_{k\text{-}\varepsilon}\le 300. \tag{15}$$

Here, y^+ is the non-dimensional distance to the wall defined by

$$y^+=u^*y/\mu, \tag{16}$$

where $u^*:=C_\mu^{1/4}k^{1/2}$ is the shear velocity. Note, that u^* is only known a posteriori and so is y^+, as these quantities depend on the flow itself. Meshing is therefore preferably done adaptively, or in practise with a good estimate of the resulting flow.

The k-ω and k-ω SST models can by themselves resolve non-fully turbulent parts of the boundary layer and therefore do not need wall functions. Their independence on these empirical relations, which are determined for some specific flow situation, but can never be guaranteed to predict the flow correctly in other situations, is positive. It puts a heavier burden on the mesh, however, as the demand for the mesh size becomes more stringent:

$$y^+_{k\text{-}\omega}\approx 1. \tag{17}$$

Figure 2. Example of an annularly corrugated tube.

This effectively means that the mesh size for a flow solved with one of the k-ω models is 50 to 300 times smaller than for the k-ε model. Note that k-ω SST uses the distance d to the nearest position on the boundary, which in addition means that the mesh should be regular near the wall.

3 EFFICIENT COMPUTATION OF THE FRICTION FACTOR

The friction factor is determined for fully developed flow. Of course, a hose has entry losses too, but these effects can be accounted for later in the design phase with correction factors. According to [13] the entry length L_e, after which a turbulent flow can be expected to be fully developed, can be approximated by

$$\frac{L_e}{D} \approx 4.4\mathrm{Re}_D^{1/6}. \tag{18}$$

For $\mathrm{Re} = 10^6$ and a hose diameter of $D = 0.5$ m, it follows that the flow in the hose reaches its fully developed stage after $L_e = 22$ m. Consequently a simulated geometry has to have at least that length. The corrugations we look at have a spacing of about 5 cm. Even without considering the specific needs for the CFD computations this means, that the mesh needs to have a resolution of one to a few millimetres on the boundary, if we want to be able to represent the boundary in detail. But doing this for 20 metres means that just to accurately represent the geometry we need 20,000 slices in length direction. If we realise that each slice has to have a fine mesh near the wall to suit the turbulence models' demands and so each slice corresponds to many thousands of points, it becomes clear that the simulation will be prohibitively costly.

Most of the information that this lengthy computation would give, would further more be discarded: we only need the the friction factor that follows from the pressure loss per metre of hose. Ideally, therefore, we would also start the computation at the point where the flow is already fully developed. We show how this can be done for annular corrugations, and then extend that method to helically corrugated hoses.

3.1 Annular corrugations

Looking at the annularly corrugated pipe in Figure 2, we can imagine that fully developed flow is somewhat different for corrugated pipes and hoses than for their smooth cousins. While in the latter we can define fully developedness as the point where the velocity no longer changes in direction and magnitude (but can be different over the cross section), for a corrugated hose that point does not exist. Since the walls of corrugated hoses have a periodic structure, we can assume that also the velocity is periodic when the flow is fully developed: the flow changes also in flow direction within a single corrugation period, but any two corrugation periods in the part of the hose where the flow is fully developed look identical:

$$\mathbf{u}(x,y,z) = \mathbf{u}(x,y,z+nL_c), \quad \forall z > L_e,\ n \in \mathbb{N}, \tag{19}$$

where we have assumed that the flow is in the z-direction and L_c is the corrugation period.

From the observation of a periodic structure of the flow, it is a small step to the wish to only compute a single corrugation period. This reduces computational costs directly by at least L_e/L_c, which for our case represents a cost reduction of a factor of the order of thousand, simply because the domain can be reduced by that amount.

Taking $z = 0$ to be anywhere in the hose where the flow can be assumed to be fully developed, we just need to perform the turbulent flow computations between $0 < z < L_c$. At the inflow and outflow side of this periodic section we simply prescribe periodic boundary conditions for most variables:

$$u(x,y,L_c) = u(x,y,0), \tag{20}$$
$$v(x,y,L_c) = v(x,y,0), \tag{21}$$
$$k(x,y,L_c) = k(x,y,0), \tag{22}$$
$$\varepsilon(x,y,L_c) = \varepsilon(x,y,0), \tag{23}$$

where k and ε can be exchanged with your favourite turbulence model variables.

Of course fully developedness does not mean that nothing is changing: to overcome friction and drag at the boundary, the pressure becomes lower each corrugation period. This makes the pressure itself non periodic. However, we can use another aspect of fully developedness, namely the fact that at each period the pressure loss of the cross section does not alter, i.e.

$$p(x,y,L_c) = p(x,y,0) + f_z L_c, \tag{24}$$

where f_z is constant for a given Reynolds number and hose geometry. Of course we have to define the value of the pressure on

at least one point; usually we set $p = 0$ in some node, e.g. at the centreline.

Not all numerical packages allow the pressure to be specified like this: if a boundary is made periodic all variables should be periodic there, the pressure too. This is quite easily surmounted by the following transformation. Split the pressure in a continuous loss due to the resistance and a local component to accommodate the variations of the geometry when corrugations are present. We already defined the pressure loss per corrugation $f_z L_c$, which means that the flow has a constant streamwise pressure gradient of f_z. Denote the fluctuations of the pressure with respect to this constant loss by p', we then can write the pressure as

$$p(x,y,z) = p'(x,y,z) + f_z z. \tag{25}$$

In the Navier-Stokes equations for incompressible flow, we only have the gradient of the pressure, so we rather use

$$\nabla p(x,y,z) = \nabla p'(x,y,z) + f_z \mathbf{e}_z, \tag{26}$$

As said, the main benefit of this reformulation is that the fluctuation pressure p' is periodic, i.e. $p'(x,y,L_c) = p'(x,y,0)$, which is usable in all numerical packages. Furthermore, this approach leads to faster/stabler convergence in all three numerical packages, that we tested: the commercial flow solver CFX, the generalist finite-element package Comsol, and the open source flow solver OpenFOAM.

The constant pressure gradient f_z can now be used in various ways. We can assume a value a priori. Using that in a numerical package we will find the flow field as a result, which enables us a posteriori determination of the Reynolds number and friction factor. Alternatively, we specify the flow field and Reynolds number and search a corresponding f_z to that. This approach fits better with the pseudo-time dependent formulation in e.g. OpenFOAM, where we adjust f_z at each timestep in order to obtain the desired Reynolds number.

For axial corrugations, of course, it is not necessary to simulate three dimensional volumes. RANS turbulence models concern averaged velocities, averaged pressure, and the turbulent energy and its dissipation are also averaged quantities. This means that these quantities are also axisymmetric if the geometry is, and that we can reduce the equations to a (quasi) two-dimensional form. For finite volume packages the use of symmetries is even simpler, instead of a part of a tube, just a single wedge of the cross section is used, where the wedge is just one cell thick. Since a wedge is typically taken at 5°, this brings another saving of a factor of a factor $360°/5° = 72$.

Note, that these steps are not allowed for more detailed models such as LES and DNS: the turbulent eddies themselves are not axisymmetric. It is a known fact that two-dimensional flows are self-organising and do not show the energy-cascade that characterises turbulence. So, if the turbulence is not modelled into other variables, reducing the equations to a two-dimensional form will eliminate turbulence from the results, and therefore make the results useless. The steps that we present are therefore only applicable for RANS models.

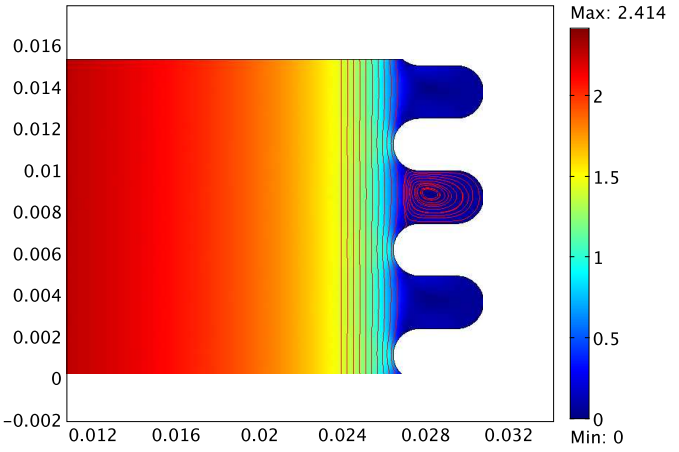

Figure 3. Velocity and selected streamlines in the Cardiff tube. All variables in SI units.

3.2 Validation of methodology

Of course we do not have measurement data for all the specific hoses, that we simulated: in fact, we carried out the simulations to minimise the number of hoses that will be experimentally tested. We therefore use a different set of pipes for validation of our methodology. The experimental results presented in [14] include friction factor measurements on a narrow metal tube of 52 mm diameter with heavy corrugations of about 6 mm deep. The measurements were furthermore done at Reynolds number well below 1,000,000. We will refer to this geometry as the Cardiff tube. Experience tells that the accuracy of RANS models increases with rising Reynolds number. We therefore expect, that we can directly see as positive results obtained for this data set as an indication for even better results at higher Reynolds numbers.

In Figure 3 the resulting velocity field is displayed. The flow is detached over the troughs of the corrugation and slowly rotating vortices exist within these corrugations. Later we will see, that the hoses of our interest can display similar behaviour.

In Figure 4 showing the fluctuating pressure $p' = p - f_z z$, we see an interesting pattern. A high pressure zone exists near the reattachment point, while a low pressure zone exists at the top of the corrugations. Their position is important: while the

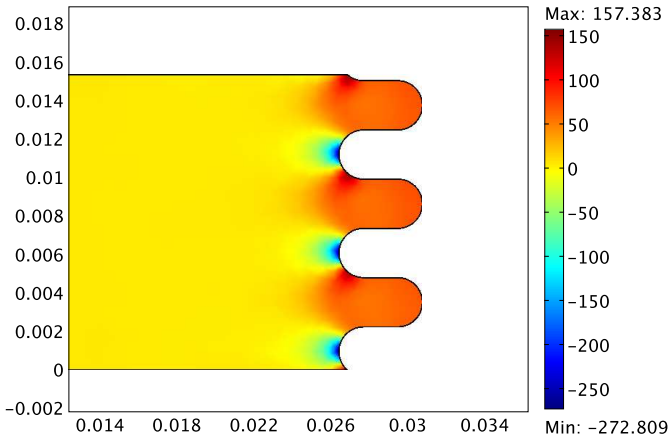

Figure 4. Periodic pressure p' in the Cardiff tube. All variables in SI units.

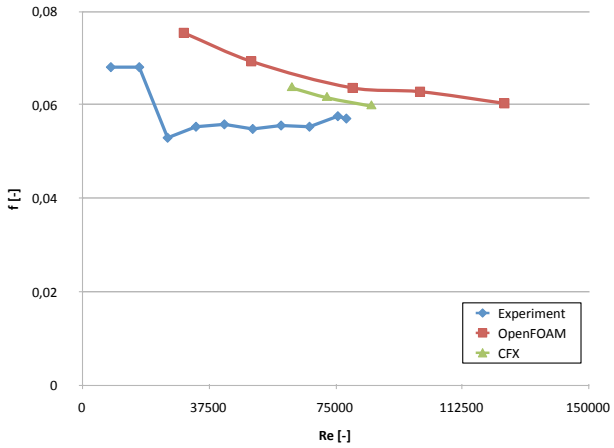

Figure 5. Friction factor computed in OpenFOAM and CFX using k-ω SST.

normal makes an angle of about 45° with the flow direction for the high pressure point, which means that the wall exerts a force that slows down the flow, the normal of the low pressure area is perpendicular to the flow, and so will not have an effect on the axial momentum. The velocity near the low pressure zone is higher which means a higher wall friction in that area. These observations indicate that the friction factor of corrugated hoses is composed of two types of forces: obviously the skin friction, which will always be higher where the corrugation protrudes the most deeply into the flow; but also the pressure on the boundary will be a significant or even dominant contributor to the hose's friction factor. Since this latter force is sensitive to the position of the reattachment point, we have arrived at the reason why large corrugations need detailed flow computations.

In Figure 5 we compare the friction factor, with respect to the tube's inner diameter, that we have computed with the measurement data of [14]. We see that the results obtained with the k-ω SST model are close to the measurements, both quantitatively and qualitatively. The methodology gives the correct results, despite the huge cost saving.

3.3 Swirl

Because the hoses that we wish to design with diameters between 10 cm and 50 cm, are much longer than L_e, up to a few hundred metres, it is inevitable that the spiral shape has an influence on the flow by intruding a swirling movement around the hose's centreline. Without directly moving to helical geometries, we can get a feel for the importance of this swirl by looking at rotating tubes.

Shchukin [15] presented measurements on rotating tubes, that show that the friction factor becomes lower as the tubes rotate faster. This is caused by the presence of a radial pressure gradient, which stabilises the flow up to the point where the laminar-turbulent transition can be shifted to much higher Reynolds numbers. Unfortunately, Shchukin's results are for near-laminar flow. To overcome the gap between this setup and out high Re problem, we have done several simulations on rotating tubes using axial symmetry and periodic boundary conditions. The simulations are not different from normal axially flowing liquid; but we have to include the azimuthal speed as an extra variable. At the boundary this speed takes the value of the rotation: $w_\Gamma = R_\Gamma \Omega$, where Ω is the rotation speed of the tube and R_Γ the distance of the boundary to the centreline of the hose.

In Figure 6 the ratio between friction factors for a rotating and non-rotating tube is drawn as a function of the non-dimensional rotational speed of the tube. We see that the behaviour is quite independent of the Reynolds number in the considered range between $4 \cdot 10^5 - -3 \cdot 10^6$. The near-laminar results of Shchukin are much milder than the high Re simulated results. The reduction of the friction factor takes the shape of a bell curve for both measured and simulated results. The swirl needs to be considerable before drag reduction becomes noticeable, but then it decays rapidly. To obtain a reduction of 10% we need $\omega D/u \approx 0.5$. Since the azimuthal speed $w = \omega D/2$, this means that $w \approx u$ for a 10% reduction. Of course it is very unlikely that the swirl will be so strong, but it indicates that swirl indeed affects the friction factor.

3.4 Helical corrugations

To make use of the helical symmetry, the Navier-Stokes equations can be rewritten in helical coordinates as done for laminar Beltrami flow in [16,17]. This leads to complicated formulations which would be hard to implement, especially since bound-

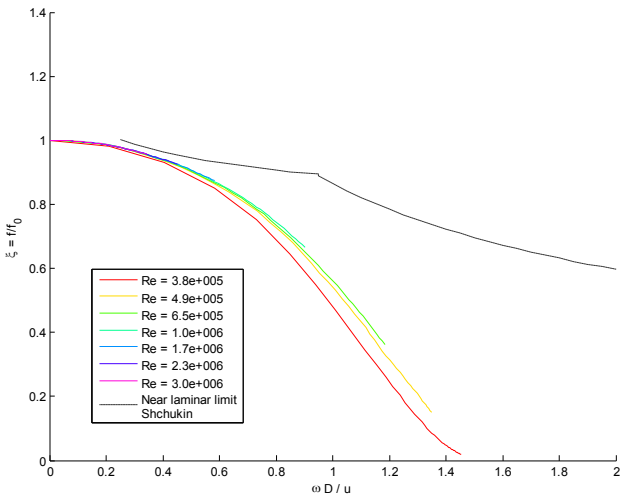

Figure 6. Friction factor reduction in rotating pipes

ary conditions for the turbulent energy and dissipation might be hard to formulate in terms of the Beltrami coordinates. For finite volume packages symmetry can easier be achieved on the mesh level by choosing a suitable section.

Helical symmetry means that the periodic variables are constant along spirals, each having the same progress per revolution. This advancement in flow direction is called the corrugation's speed L_c. Expressed in cylindrical coordinates (r,φ,z), the speed for example has this structure:

$$\mathbf{u}(r,\varphi,z) = \mathbf{u}(r,\varphi+\Delta\varphi,z+\frac{L_c}{2\pi}\Delta\varphi), \quad \forall\Delta\varphi\in\mathbb{R}, \tag{27}$$

where L_c is speed of the corrugation, i.e. the advancement in flow direction after going around the hose once. The same equation can be used for the other periodic variables: p', k, ε and ω.

A direct application of (27) would work in the same way as a 3D smooth tube mesh might be constructed:

1. Generate a cross section of the corrugated tube in a CAD program;
2. Generate a two-dimensional mesh on this cross section;
3. Extrude this mesh in z-direction over a length L_c while rotating the mesh 360°.

In Figure 7 we show the resulting mesh. Since we made a full revolution, we can use the same periodic boundary conditions on the top and bottom of this disc. Un fortunately if we zoom into the boundary we immediately see this method's drawbacks: for small helical angles $\vartheta_c = \arctan L_c/(\pi D)$ this method will generate elements with two corners of that size and two very obtuse corners at $\pi/2-\vartheta_c$. The elements at the boundary are not

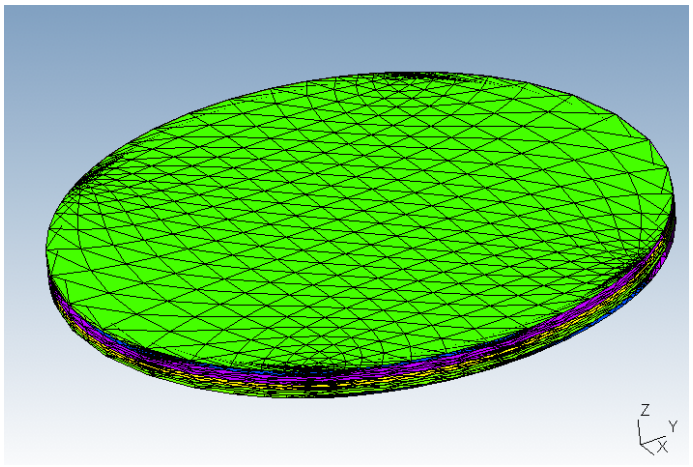

Figure 7. Helical mesh obtained by twisting extrusion of its cross section.

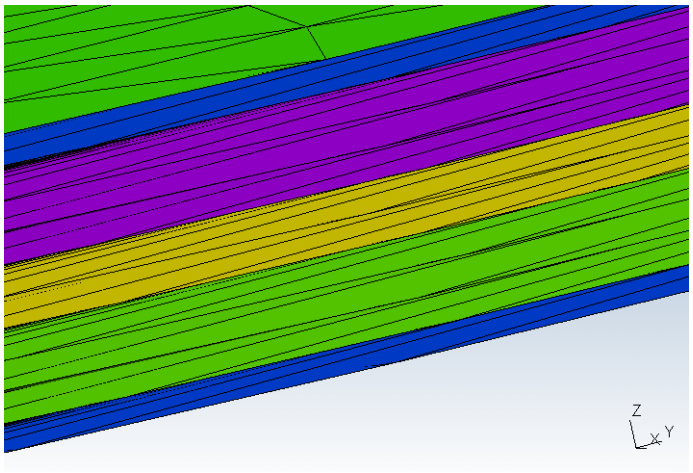

Figure 8. Bad elements near the boundary for cross-sectional extrusion

aligned with the flow and will also for that reason produce poor numerical results. Another drawback is that the 3D shape is very sensitive to errors in the original outline.

Fortunately, we can choose any plane to start from. For small corrugation angles, it is better to start from a section in the r-z plane, e.g. at $\varphi = 0$. We choose a section that holds single or multiple periods of the corrugation and perform the same extrusion with rotation. The resulting mesh can be seen in Figure 9. Here, we have to apply two different sets of periodic boundary conditions. Since we made a full revolution, the top and bottom can still be prescribed as before, even if these surfaces now are curved. Since the mesh does not meet up with the start after a full revolution, the two sections which are on top of each other in the $\varphi = 0$ plane. Because these are in the same plane, no rotation of vector quantities such as the speed needs to be done.

Note that this method creates degenerate cells if they have

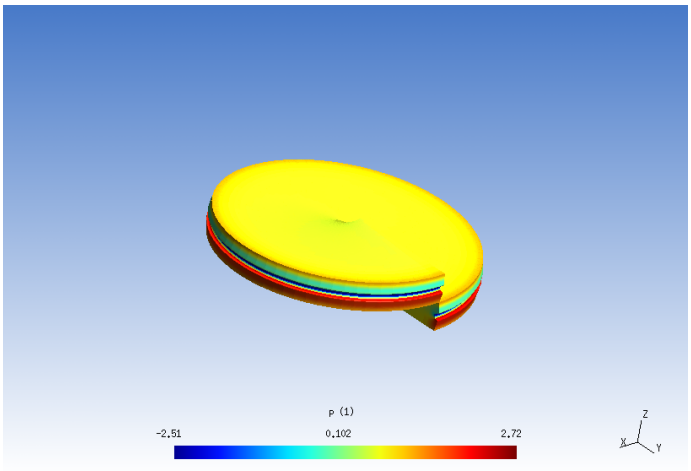

Figure 9. Periodic pressure p' in a Beltrami-symmetrical mesh.

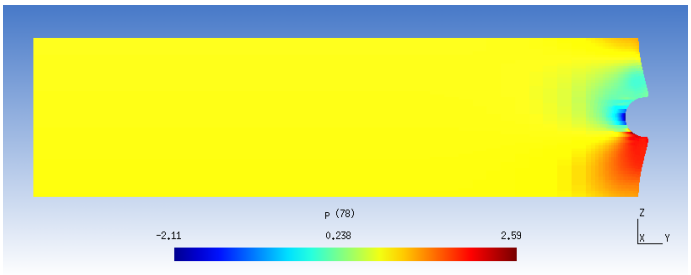

Figure 10. Periodic pressure p' in a axisymmetric mesh.

points on the axis of rotation. If the underlying numerical program cannot deal with these elements, the solution is to start with a two-dimensional mesh in the r-z plane that does not include $r = 0$. A narrow cylinder will then be left out of the 3D mesh. If a slip boundary condition is applied to the surface of that cylinder, the result will be nearly identical to the real solution.

Figure 9 also shows the resulting pressure after a computation with the k-ω SST model in OpenFOAM. Because the swirl is small, the pressure distribution is not very different from a similar but axisymmetric computation shown in Figure 10. The friction factors, too, do not vary much at $\mathrm{Re} = 10^6$. The axisymmetric, swirl-less friction factor is $f = 0.005948$ while the helical geometry with the small swirl yields the less than one percent lower $f = 0.005917$. So, while the swirl does have an effect, at these high Reynolds numbers and small corrugation angles, the effect is not significant enough to justify the extra computational time.

4 DISCUSSION

In this paper we have shown how to efficiently compute friction factors using CFD tools. By making use of the periodicity of the fully developed flow, we only need to compute a single

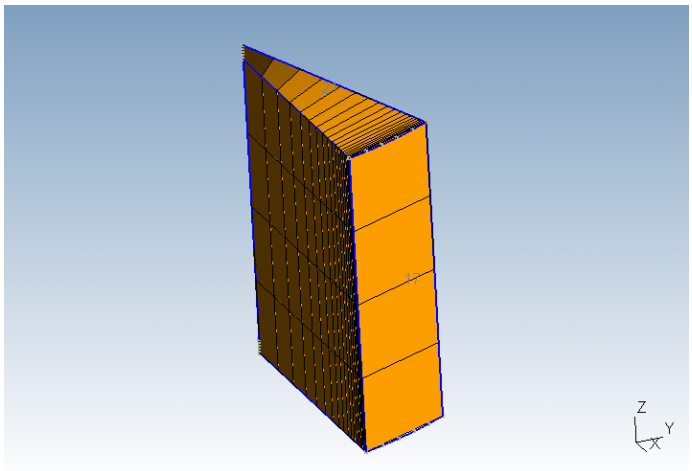

Figure 11. Example of a Beltrami wedge. Note the curved surface on top and (not visible) bottom.

corrugation period. Since corrugation lengths are typically much smaller than the entry length of the hose, which otherwise would have to be included to arrive at the fully developed state of the flow, this leads to an enormous saving. For the hoses we are interested in computing it approaches a factor 1,000.

For the axisymmetric case, we only need to compute a single wedge, which saves another factor 72 in computational effort, bringing the total time saving near to a factor 100,000. For helical symmetries this extra saving would also be feasible, if one were to use a distorted wedge as shown in Figure 11. This wedge is created in the same way as Figure 9, but rather than twisting a full 360° around the hose's centreline, only a rotation of 5° is made, as we do for the axisymmetric case. Prescribing the periodic boundary condition for a single wedge becomes more complicated, however, as vector quantities (velocity) need to be properly rotated before they can be equated. The difference between axisymmetry and Beltrami-symmetry is so small for small corrugation angles, that we have not seen this as worth the effort.

5 CONCLUSION

Using the presented methodology, the computation of the friction factor can be done reliably in a matter of minutes. This means that not only can we consider a wide variety of hoses, we can even actively optimise the design of the hose, by adjusting several geometric characteristics of the hose. In Figures 12 and 13 two different corrugations are shown. By adjusting the shape of the tissue between two corrugations, the position of the stagnation point can be adjusted, and the friction factor can thus be influenced. Thanks to the speed up of computation, the optimisation can even be done automatically.

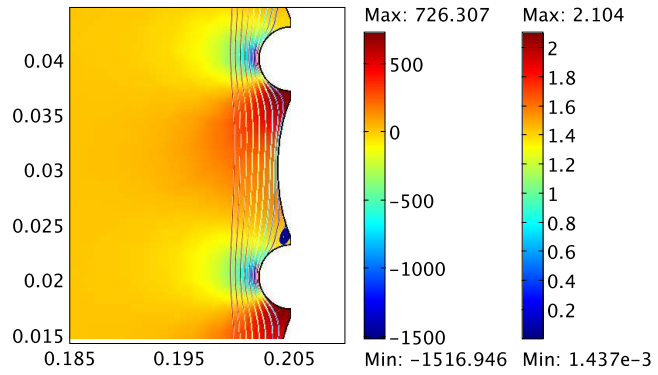

Figure 12. Hose with tight outer spiral and protruding secondary corrugation.

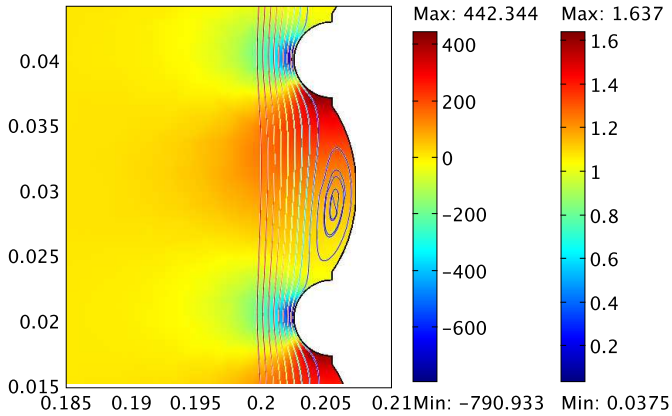

Figure 13. Hose with loose outer spiral and hollow secondary corrugation.

REFERENCES

[1] Altunin, V. I., 1977. "Hydraulic resistance of corrugated pipes". *Gidrotekhnicheskoe Stroitel'stvo*(9), September, pp. 32–36.

[2] Moody, L. F., 1944. "Friction factors for pipe flow". *Trans. ASME,* **66**(8), November, pp. 97–107.

[3] Romeo, E., Royo, C., and Monzón, A., 2002. "Improved explicit equations for estimation of the friction factor in rough and smooth pipes". *Chemical Engineering Journal,* **86**, pp. 369–374.

[4] Pope, S. B., 2000. *Turbulent Flows*. Cambridge University Press, Cambridge, UK.

[5] Blazek, J., 2001. *Computational Fluid Dynamics: Principles and Applications*. Elsevier, Amsterdam, The Netherlands.

[6] Jones, W. P., and Launder, B. E., 1972. "The prediction of laminarization with a two-equation model of turbulence". *Int. J. Heat Mass Transfer,* **15**(2), pp. 301–314.

[7] Pisarenco, M., van der Linden, B. J., Tijsseling, A. S., Ory, E., and Dam, J., 2009. "Friction factor estimation for turbulent flows in corrugated pipes with rough walls". In Proceedings of the ASME 28th International Conference On Ocean Offshore and Artic Engineering, no. OMAE2009-79854.

[8] Wilcox, D. C., 2006. *Turbulence Modeling For CFD, 3rd ed.* DCW Industries, Inc., La Cañada, California.

[9] Thivet, F., Daouk, M., and Knight, D. D., 2002. "Influence of the wall condition on k-ω turbulence model predictions". *AIAA Journal: Technical Notes,* **40**(1), pp. 179–181.

[10] Menter, F. R., 1992. Improved two-equation k-ω turbulence models for aerodynamic flows. Technical Memorandum 103975, NASA, October.

[11] Celić, A., and Hirschel, E. H., 2006. "Comparison of eddy-viscosity turbulence models in flows with adverse pressure gradients". *AIAA Journal,* **44**(10), October, pp. 2156–2169.

[12] Zuckerman, N., and Lior, N., 2005. "Impingement heat transfer: Correlations and numerical modelling". *J. Heat Transfer,* **127**, pp. 544–552.

[13] White, F. M., 2000. *Fluid Mechanics, 4th edition*. WCB McGraw-Hill, Boston, Mass.

[14] Marsh, R., and Griffiths, T., 2006. Pressure loss in cooling hoses. Tech. Rep. 3121, Cardiff University, School of Engineering, UK.

[15] Shchukin, V. K., 1967. "Hydraulic resistance of rotating tubes". *Inzhenerno-Fizicheskii Zhurnal,* **12**(6), pp. 782–787.

[16] Dritschel, D. G., 1991. "Generalized helical Beltrami flows in hydrodynamics and magnetohydrodynamics". *J. Fluid Mechanics,* **222**, pp. 525–541.

[17] Landman, M. J., 1990. "Time-dependent helical waves in rotating pipe flow". *J. Fluid Mechanics,* **221**, pp. 289–310.

PREVIOUS PUBLICATIONS IN THIS SERIES:

Number	Author(s)	Title	Month
09-12	L.M.J. Florack	Coarse-to-fine partitioning of signals	March '09
09-13	J.A.W.M. Groot C.G. Giannopapa R.M.M. Mattheij	Numerical optimisation of blowing glass parison shapes	March '09
09-14	A.S. Tijsseling	Exact computation of the axial vibration of two coupled liquid-filled pipes	May '09
09-15	M. Pisarenco B.J. van der Linden A.S. Tijssseling E. Ory J.A.M. Dam	Friction factor estimation for turbulent flows in corrugated pipes with rough walls	May '09
09-16	B.J. van der Linden E. Ory J.A.M. Dam A.S. Tijsseling M. Pisarenco	Efficient computation of three-dimensional flow in helically corrugated hoses including swirl	May '09

Ontwerp: de Tantes,
Tobias Baanders, CWI